Pion emission in ^{2}H,^{12}C,^{27}Al(γ,π^{+}) reactions at threshold

P. Golubev [a], V. Avdeichikov [a], K.G. Fissum [a], B. Jakobsson [a,*], I. A. Pshenichnov [b,c], W. J. Briscoe [d], G. V. O'Rielly [e], J. Annand [f], K. Hansen [g], L. Isaksson [a,g], H. Jäderström [h], M. Karlsson [a], M. Lundin [g], B. Schröder [a], L. Westerberg [i],

[a] *Dept. of Physics, Lund University, Box 118, SE 221 00 Lund, Sweden*

[b] *Frankfurt Inst. for Advanced Studies, J.W. Goethe University, 60438 Frankfurt am Main, Germany*

[c] *Inst. for Nuclear Research, Russian Academy of Science, 117312 Moscow, Russia*

[d] *The George Washington University, Washington, DC 20052 USA*

[e] *University of Massachusetts Dartmouth, North Dartmouth, MA 02747 USA*

[f] *Dept. of Physics, University of Glasgow, UK*

[g] *MAX-lab, Lund University, Ole Römers väg 1, Lund, Sweden*

[h] *Dept. of Nuclear and Particle Physics, Uppsala University, Box 535, SE 751 21 Uppsala, Sweden*

[i] *Dept. of Physics, Uppsala University, Box 530, SE 751 21 Uppsala, Sweden*

Abstract

The very first data from MAX-lab in Lund, Sweden on pion photoproduction at threshold energies are presented. The decrease of the total π^{+} yield in γ + ^{12}C, ^{27}Al reactions below 200 MeV as well as the dσ/dΩ cross-section data essentially follow the predictions of an intranuclear-cascade model with an attractive potential for the pion-nucleus interaction. However, d$^{2}\sigma$/dΩdT, cross-section data at 176 MeV show deviations which call for refinements of the model and possibly also for the inclusion of coherent pion-production mechanisms.

Key words: Photonuclear reactions; π^{+} emission; Threshold energies; Range telescope technique; Intranuclear cascade model;
PACS: 25.20.Lj, 25.75.Dw

* Corresponding author: Bo.Jakobsson@nuclear.lu.se

1 Introduction

Studies of (γ, π) reactions on nuclei provide information on the in-medium pion-nucleon (πN) interaction [1,2], the properties of excited spin-isospin flip states of residual nuclei [3,4] and the properties of few-body systems [5]. A proper theoretical description of photonuclear reactions and in particular of pion photoproduction on nuclei, is a prerequisite for calculations performed for the photodisintegration of ultra-high energy nuclei in the cosmic microwave background [6] and on nuclear fragmentation reactions induced by virtual photons [7].

Unfortunately, data on nuclear pion photoproduction are scarce in the near-threshold region because of lack of relevant photon beams. The recently upgraded nuclear-physics beamline at MAX-lab is one of only a handful of facilities worldwide which can now provide a photon beam of appropriate energy. This is done by colliding a pulse-stretched electron beam [8,9] with a thin radiator and momentum analyzing the post-bremsstrahlung electrons in one of two tagging spectrometers [10]. That said, for the early measurements reported on in this paper, the tagging spectrometers were not yet commissioned. Thus, in this untagged experiment, the photon-endpoint energy was 189 MeV and the average photon-beam energy was estimated to be 176 $\pm$ 2 MeV (see section 2.6).

Some data on near-threshold pion production exist [3,4,11] but these come mainly from experiments with rather high pion detection thresholds. In this experiment, the two range telescopes allowed for a relatively low threshold for pion detection (8.4 and 8.7 MeV) which was achieved using a thin (3 mm) first plastic detector and a compact telescope design. Unfortunately, the limited solid-angle coverage and the fact that the absolute normalization of the data reported on here utilizes (γ,p) cross-sections from the literature result in large statistical and systematic uncertainties.

The measured total cross-section data for π^+ photoproduction on ^{2}H, ^{12}C and ^{27}Al, together with the corresponding differential ($\mathrm{d}\sigma/\mathrm{d}\Omega$) and double differential ($\mathrm{d}^2\sigma/\mathrm{d}\Omega\mathrm{d}T$) cross-section data have been compared with results from the RELDIS Monte Carlo model for photonuclear reactions [12,13]. In this model, the quasi-deuteron absorption mechanism coexists with quasifree meson photoproduction on individual nucleons.

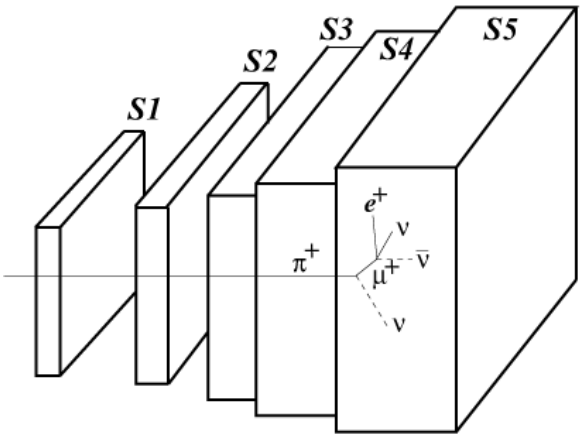

Fig. 1. Principle geometry and π^+ detection process in the range telescopes (not to scale).

2 Experimental details

2.1 Photon beam and targets

The stretched electron beam from the MAX I ring [8] has long been used for photonuclear experiments at the Tagged-Photon Facility at MAX-lab. As previously mentioned, in this, very first (γ, π) experiment, the tagging spectrometers [9] were not in operation. The electron beam was simply passing through a 150 μm thick Al radiator which produced a photon beam with bremsstrahlung energy distribution in the interval 0 - 189 MeV. These photons passed through a 19 mm diameter collimator before impinging on experimental targets of C, CD_2 and Al with thickness 1 - 2 mm. All results on γ + ^{2}H reactions have been determined from the data on C and CD_2 targets.

2.2 Pion detectors

The technique used to identify π^+ in this experiment was based on measuring the 26 ns $\pi\mu$ decay in plastic scintillator range telescopes (Fig. 1). The efficiency for identifying pions depends here mainly - but not solely - on telescope geometry. It was important to minimize both the electronic noise through proper grounding and the room background through concrete shielding. After such precautions, we found that plastic scintillator telescopes of the CHIC design [14] were very effective at selecting pions.

Consequently, two telescopes of this type were designed for the experiment under the assumption of an effective upper limit in pion energy well below 50 MeV. Each telescope was comprised of five NE102 plastic scintillators (S_1 - S_5), which were read out by Philips XP2020 photomultipliers (PMTs). Table 1 presents the geometries chosen for the telescopes and the resulting energy bins for protons and pions that stop in each of the detector elements. Since pion identification required at least two energy signals (see below), the low-energy limit for pion detection was set essentially by the thickness of element S_1. Including the minor energy loss that pions experience in target material, air and wrapping of the scintillators (which is different for the two telescopes), the detection thresholds for pions were 8.4 ± 0.1 MeV and 8.7 ± 0.1 MeV for the 30° and 90° telescopes respectively. The maximum pion energies each telescope could stop were 57.5 MeV and 49.9 MeV, respectively. The fact that one single pion was registered in each of the two last (S_5) detectors shows that the choice of telescope thicknesses was reasonable.

Table 1
Telescope geometry (th = thickness) together with the proton and pion energy bins (T_p, T_π) for the telescopes.

	90° telescope				30° telescope			
det.	th (mm)	area (mm^2)	T_p (MeV)	T_π (MeV)	th (mm)	area (mm^2)	T_p (MeV)	T_π (MeV)
S_1	3	60·60	0 - 17.2	0 - 8.7	3	60·60	0 - 16.8	0 - 8.4
S_2	5	85·85	17.2 - 29.1	8.7 - 13.8	5	70·70	16.8 - 28.9	8.4 - 13.3
S_3	20	90·90	29.1 - 57.7	13.8 - 26.2	10	80·80	28.9 - 45.2	13.3 - 20.4
S_4	30	95·95	57.7 - 86.4	26.2 - 38.8	20	90·90	45.2 - 68.3	20.4 - 30.2
S_5	50	100·100	86.4 - 122.6	38.8 - 57.5	50	100·100	68.3 - 109.2	30.2 - 49.9

2.3 Electronics and data acquisition

In order to identify π^+, the PMT anode signal of each detector was split and sent to two independent charge integrating ADCs with individually adjustable gates. The "prompt-gated" ADC had a 100 ns long gate which was open for integration 5 ns before the analogue PMT signal appeared. The "delay-gated" ADC, also had a 100 ns long gate, which was opened when the largest amplitude of the analogue pulse was reached. This opening time was individually adjusted from the proton pulses, easy to recognize with beam on target.

For each master trigger which required signals in the first two detector elements, S1*S2, the hit-pattern was registered and stored in ROOT-tree files together with all the ADC and TDC information. A local, VME based data acquisition system was used for this storage.

2.4 Pion identification

Figure 2 presents typical on-line data. The upper plot shows the prompt ΔE - E correlation (in this case, S_2 vs S_3 in the 30° telescope) after the ADC and TDC patterns have been used to identify the detector element in which the pion stopped. No other constraints have been imposed. The existence of three groups of particles - protons, pions and e-γ background - is obvious. It is important to note that the PMT gains were set so that all protons were registered (see section 2.6).

The pion band contains both π^+ and π^-. π^+ were then selected in the E_{prompt} vs. E_{delay} plots for the "stop" detector (Fig. 2 - mid). The muon from the $\pi^+ \rightarrow \mu^+\nu$ decay (nearly 100% branching ratio) can be detected with a certain efficiency (see section 2.5). The π^- is normally absorbed by a carbon atom of the scintillator and it thus appears in the E_{prompt} - E_{delay} plot either in the lower band if only neutral particles are emitted from the disintegrating carbon nucleus or in a random background position if charged particles are emitted. Selecting the upper band in Fig. 2 (mid) thus provides clean π^+ identification as evidenced by Fig. 2 (lower), which shows only those events originally present in Fig. 2 (upper) which pass the π^+ identification.

Pion-energy intervals were defined from the energy-range intervals that stopped pions have in the detectors (Table 2). Polynomial fits, to the energy distributions, using the detector half thicknesses were then used to determine the final energies. This resulted in systematic uncertainties of $\sim \pm 1$ MeV in the pion energies. Note that linear scintillator response functions have been used when pion detection thresholds are artificially introduced in software.

2.5 Determination of the π^+ detection efficiency

The number of π^+ obtained in the three-step analysis process described above was corrected for the following processes:
i) pion decay in flight.
ii) nuclear reactions in the target and detector material.
iii) sliding trajectories (detector geometry).
iv) μ^+ detection efficiency.

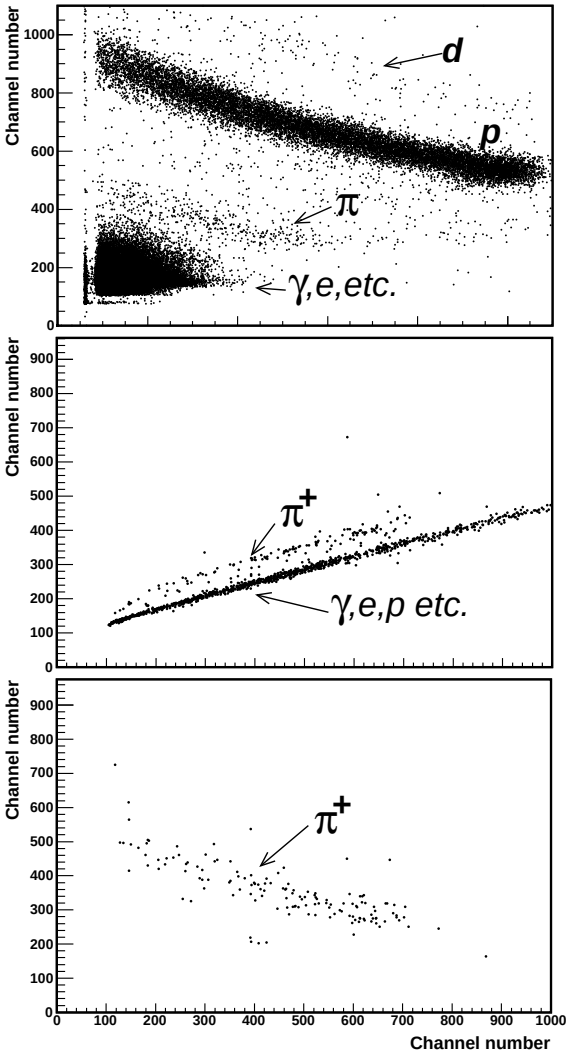

Fig. 2. (Upper) Prompt ΔE - E plot for particles stopping in the S_3 detector of the 90° telescope. (Mid) Delayed vs. prompt ADC signals for events lying in the pion band in the upper plot. (Lower) Prompt ΔE - E plot revisited, now for those events defined as π^+ in the middle plot.

The first three processes make pions undetectable, while correction iv) accounts for losses of π^+ in the E_{prompt} - E_{delay} plot when muons leave the stop detector before decaying ($\mu^+ \rightarrow e^+ \nu\bar{\nu}$). In the efficiency calculations, it was assumed that half of the muon energy ($0.5 \cdot 4.2$ MeV) must be deposited in the detector for the pion to appear in the proper band in the E_{prompt} - E_{delay} plot. All effects have been calculated analytically following the procedure in Ref. [14] and also by Monte-Carlo simulations using GEANT4 [15]. Table 2 shows the results. Note that the analytically determined, total corrections (ranging from 24 to 44%) are systematically lower than the results from the

Monte-Carlo simulations (32 - 69%). This difference is interpreted to result from approximations in the analytic scattering kinematics calculations. The larger correction factors resulting from the simulations were thus used to obtain the true number of photopions. The differences in the corrections were the main contributions to the systematic uncertainties in the detection efficiency (see section 2.7).

Table 2
Total correction factors for detector efficiency in the elements S_2 to S_5 calculated analytically and simulated with GEANT4 (see text for details).

	α (90^0) telescope		β (30^0) telescope	
Det.	Analytic corr.	M-C corr.	Analytic corr.	M-C corr.
S_2	1.44	1.69	1.44	1.69
S_3	1.31	1.48	1.33	1.54
S_4	1.28	1.39	1.30	1.42
S_5	1.24	1.32	1.26	1.37

2.6 Normalization and average beam energy

Because of the low data acquisition rate, $\ll 1{\cdot}10^3$ events/s, no proton rejection was necessary. Consequently, the registered protons could be used for absolute normalization. A mixture of inclusive and semi-exclusive (γ,p) cross-sections have been utilized for this normalization [16,17,18,19,20].

The fundamental, triple differential cross-section that was extracted from this experiment is,

$$\frac{d^3\sigma_{\pi,p}}{dE_\gamma d\Omega_{\pi,p} dT_{\pi,p}}(E_\gamma, \Theta_{\pi,p}, T_{\pi,p}) = \frac{1}{C_{\pi,p}} \cdot \frac{1}{\Phi_o(E_\gamma)} \cdot \frac{N_{\pi,p}(E_\gamma, \Theta_{\pi,p}, T_{\pi,p})}{\Delta E_\gamma \Delta\Omega \Delta T_{\pi,p}}, \quad (1)$$

where $T_{\pi,p}$ and $\Theta_{\pi,p}$ are the kinetic energy and emission angle of protons and pions respectively. $C_{\pi,p}$ are the normalization constants (which depend on target mass number, thickness and density) and $\Phi_o(E_\gamma)$ is the bremsstrahlung spectrum of incident photon energies. $N_{\pi,p}$ is the efficiency-corrected pion(proton) yield. $\Delta\Omega$ is the solid angle subtended by the detector. The most extensive (γ,p) data were found for photon collisions on ^{12}C. Total, inclusive cross-sections could in this case be found at energies $\geq$ 200 MeV [16] while total cross-sections at lower energies must be estimated from missing energy biased data [17]. The normalization constant C_p was obtained from the number of protons registered in all of the stop detectors, $\sum_{E_\gamma=0}^{189} \sum_{T_p=17}^{T_{p,max}} N_p(E_\gamma, \Theta_p, T_p)$ and the empirical triple differential cross-section integrated over the proper

intervals in E_γ and T_p. In practice, a polynomial fit to the function $f(E_\gamma) = \int_0^{189} \Phi_o(E_\gamma) \cdot \int_{17}^{T_{p,max}} \frac{d^3\sigma}{dE_\gamma d\Omega_p dT_p}(E_\gamma, \Theta_p, T_p) dE_\gamma dT_p$ was extracted.

If the pion triple differential cross-section had been known, $C_\pi = k \cdot C_p$ could be determined in a similar manner (and ideally k = 1). Instead, an ansatz was made by extrapolating a polynomial fit to the Fissum et al. data [11] (photon energy region 184 - 213 MeV) to an energy of 160 MeV, below which the pion contribution was neglected. C_π was then calculated in the same way as C_p. Thus, a polynomial function was fitted to $g(E_\gamma) = \int_0^{189} \Phi_o(E_\gamma) \cdot \int_{17}^{T_{\pi,max}} \frac{d^3\sigma}{dE_\gamma d\Omega_\pi dT_\pi}(E_\gamma, \Theta_\pi, T_\pi) dE_\gamma dT_\pi$. The number of pions includes here only those with $T_\pi > 17$ MeV, efficiency corrected accordingly (Table 1). As mentioned before (section 2.4), linear scintillator response functions were assumed when fractions of "stop" detector energy bins were introduced. In a typical example of this procedure the determination of absolute differential cross-sections for $\gamma + ^{12}C$ at 90° k was determined to 0.79 with an uncertainty of 15% (see section 2.7).

The same procedure was carried out for the $\gamma + ^{27}$Al and $\gamma + ^{2}$H reactions. Because of the limited number of "normalizing" data, available for $\gamma + ^{27}$Al, also $\gamma + ^{40}$Ar data were used to guide the A_T dependence of C_π.

The ansatz for the $g(E_\gamma)$ function resulted in $< E_\gamma > = 178 \pm 2$ MeV for pion producing events. Introducing the data from this work at 178 MeV photon energy, resulted in a decrease of $< E_\gamma >$ to 176±2 MeV. Further recursive iterations along this line changed the value by < 1 MeV. The $< E_\gamma >$ was consequently fixed at 176±2 MeV. Within the limits of uncertainty, the average photon energy was the same for all three $\gamma + ^{27}$Al, ^{12}C,^{2}H reactions.

2.7 Systematic and statistical uncertainties

Statistical uncertainties only are presented with the data in Figs. 3 - 7 with two exceptions - the two upper points (triangles) in Fig. 4. These contain the yield of pions with energy below the detector cutoff, which has been extrapolated both from data and RELDIS calculations. The extrapolated yields contribute with 30% and 50% of the differential cross-sections at 30° and 90° lab angle respectively. The uncertainties of these yields, which are introduced in the error bars of the two points in Fig. 4, are set to 30 %, based on the difference between the empirical and RELDIS extrapolations.

Three major sources of systematic uncertainties in eq. (1) were identified. First, the systematic uncertainty in the detector efficiency has been taken as the difference in the results obtained from the analytic and Monte-Carlo calculations. This gives a pion-energy dependent uncertainty ranging from

7% at high energy to 17% at low energy (Table 2). The second source of uncertainty comes from the manner in which the cuts identifying the pion yield was applied. This uncertainty was estimated to be $\sim 9\%$. The third systematic uncertainty enters via C_p through its dependence on the (γ,p) cross-section data taken from the literature. By comparing the pion yields from the γ + ^{12}C reaction that are obtained with and without the use of the data from Ref. [16] to estimate C_p, this uncertainty was determined to be 12%. Other sources of uncertainty were negligible. This resulted in total systematic uncertainties for the γ + ^{12}C reaction that range from 17% at the highest pion energy to 23% at the lowest. The uncertainties are somewhat larger (up to 28%) for the other two reactions.

3 The RELDIS model for photonuclear reactions

Below pion production threshold, at $E_\gamma \sim 140$ MeV, the de Broglie wavelength λ is comparable to the distance between nucleons in nuclei and photon absorption by a quasi-deuteron is the main reaction mechanism. At higher energies (as λ becomes comparable to the nucleon radius), photons interact mainly with single nucleons, thereby exciting baryon resonances and producing mesons. The RELDIS model takes into account these two competing channels. Here, the input to the code relevant for photon energies close to the pion production threshold is described. More details can be found in Refs. [12,13].

3.1 Calculation of quasi-deuteron absorption

The two-nucleon photoabsorption cross-section on a heavy nucleus $\sigma_{\gamma A}^{QD}$ is taken from the quasi-deuteron model of Levinger [21], as modified in Ref. [22],

$$\sigma_{\gamma A}^{QD} = kZ(1 - Z/A)\sigma_d^{exch}. \quad (2)$$

Here σ_d^{exch} is the meson-exchange part of the cross-section σ_d for deuteron photodisintegration, $\gamma d \rightarrow np$ [23], A and Z are the mass and charge numbers of the target nucleus and $k \approx 11$ is an empirical constant taken from the analysis of Ref. [22].

The cross-section $\sigma_{\gamma A}^{QD}$ decreases strongly with photon energy. Nevertheless, the two-nucleon absorption mechanism competes noticeably with the single-nucleon absorption up to $E_\gamma \sim 0.5$ GeV.

3.2 Simulation of pion photoproduction on nucleons in a nucleus

The main single-nucleon photoabsorption mechanism is meson production. The two-body channel $\gamma N \rightarrow \pi N$ dominates up to $E_\gamma \sim 0.5$ GeV. This process was calculated in the framework of the phenomenological approach of Ref. [24,25]. In this approach, the pion photoproduction amplitude contains Breit-Wigner resonant terms, Born terms and a weakly energy-dependent "background" contribution. The latter was used as an adjustable parameter. Masses and widths of the resonances were taken from πN-scattering data, with their amplitudes taken as free parameters. The excitation of six different baryon resonances were considered with the $\Delta(1232)$, $N^\star(1520)$ and $N^\star(1680)$ resonances the most important of them.

Tables of total reaction cross-section data together with photopion angular distributions calculated according to Refs. [24,25] were taken from Ref. [26].

Both the total and the differential cross-sections of the $\gamma p \rightarrow \pi^+ n$, $\gamma n \rightarrow \pi^- p$ and $\gamma p \rightarrow \pi^0 p$ processes are well described by the γN Monte Carlo event generator [12] used by the RELDIS model. Presently, the γN event generator used in the RELDIS model extends the event generator by Corvisiero et al. [26] to higher photon energies (up to 10 GeV) and multiple pion production, as demonstrated in Refs. [12,13].

3.3 Secondary interactions of photohadrons

Hadrons produced in a primary γN or $\gamma d \rightarrow np$ interaction initiate a cascade of successive hadron-nucleon collisions inside the target nucleus during the cascade stage of the photonuclear reaction. Calculations are based on a Monte Carlo technique used to solve the equation that describes hadron transport in the nuclear medium. The target nucleus is considered to be a mixture of degenerate Fermi gases of neutrons and protons in a spherical potential well with a diffuse boundary. By using the effective real potentials for nucleons and pions, the influence of the nuclear medium on cascade particles is taken into account. It should be stressed that this potential is taken to be constant although it should depend on the nuclear density as well as on the pion kinetic energy. However, it is beyond the scope of the present experiment to provide the very precise data necessary to tune these dependences.

The momentum distributions of nucleons in the nuclei are calculated in the local-density approximation of the Fermi-gas model. The distribution of nuclear density is approximated by a set of step functions for the nuclear radius. The Coulomb potentials for charged cascade particles are calculated for each density zone.

The cross-sections for pion interactions such as $\pi N \rightarrow \pi N$, $\pi(NN) \rightarrow NN$, $\pi N \rightarrow \pi\pi N$ etc, as well as nucleon-induced processes, $NN \rightarrow NN$, $NN \rightarrow \pi NN$, ,... etc in the nuclear medium are assumed to be the same as in vacuum, except that the Pauli principle prohibits the transition of the cascade nucleons into states already occupied.

4 Experimental data and comparison to RELDIS calculations

Data on π^+ cross-sections were measured in the T_π interval(s) 8.7(8.4) - 57.5(49.9) MeV. No pions with higher energies are expected (section 2.2). For simplicity, these pions are subsequently denoted as $T_\pi > 9$ MeV pions. Due to limited statistics, data points are presented one per "stop" detector (Table 1), all at beam energy $E_\gamma = 176$ ($\pm$ 2) MeV (recall section 2.6).

In the near-threshold RELDIS simulations used for comparison to the data in Figs. 3 - 7, the only process for π^+ production is $\gamma p \rightarrow \pi^+ n$. Photopions can then face elastic scattering from nucleons in the target nucleus, charge-exchange reactions (such as $\pi^+ n \rightarrow \pi^0 p$) or absorption on two nucleons. The key parameter in these simulations is the real part of the pion potential V_π which is assumed to be attractive, $V_\pi < 0$. This potential is taken as an empirical parameter, independent of the pion energy. Its value has been derived from pion production data reasonably close to threshold. The imaginary part of the pion potential is simulated by taking into account the pion absorption reaction $\pi(NN) \rightarrow NN$.

Because of the limited statistics and large systematic uncertainties, it is difficult to compare the double differential cross-section data to the predictions from RELDIS, which themselves are very sensitive to small changes in the input parameters. Therefore, total (energy and angle integrated) cross-section data are presented and discussed first. Least squares fits to Boltzmann functions (energy) and polynomial functions (angular) have been introduced to carry out these integrations.

4.1 Total yield of π^+

Data from Ref. [11] demonstrate a falloff of σ_{π^+} with decreasing E_γ towards the effective reaction threshold. The measured total cross-section data for pions with $T_\pi > 17$ MeV (the cutoff in Ref. [11]) from this experiment and from selected parts of Ref. [11] are shown in Table 3. The average systematic uncerainty in the ^{1}H and ^{12}C data from Ref. [11] was $\sim$ 17%, i.e. somewhat less than in the present experiment (see Table 3).

Table 3
Total cross-section data for π^+ photoproduction with $T_\pi > 17$ MeV from this work and from Ref. [11]. Statistical uncertainties are shown.

	$\sigma(\mu b)$				
E_γ (MeV)	^{1}H	^{2}H	^{12}C	^{27}Al	^{40}Ca [a]
176 (this work)	-	0.8±0.2 [b]	7.2±1.2 [c]	43±7 [d]	-
184 [11]	-	-	31.1±2.0	-	131.8±7.8
194 [11]	82.0±3.7	-	64.4±2.8	-	177.8±11.7
204 [11]	92.3±4.2	-	107.8±3.8	-	354.3±13.0
213 [11]	103.7±4.7	-	160.7±4.5	-	498.1±15.0

[a] Systematic error associated with the background 8.8 μb [11]
[b] Systematic error 0.2 μb, [c] Systematic error 1.4 μb, [d] Systematic error 12 μb

The process that RELDIS uses to produce pions should result in σ_{π^+} scaling with Z_{target}. Thus, σ_{π^+} / Z_{target} vs. E_γ is plotted in Fig 3. The Fissum et al. data show that heavy nuclei are less efficient in photoproducing pions. This may be due to the enhanced reabsorption of π^+. The strongest deviation from Z_{target} scaling appears actually in the γ + ^{1}H cross-section, which is 5 - 10 times more efficient in producing π^+ than the γ + nucleus reactions [11].

The new data shown in Fig. 3 exhibit an enhanced falloff of pion production in the γ + ^{12}C reaction, consistent with the predictions of the RELDIS model. There is of course a shift from the (γ, N) channel to the quasi-deuteron absorption channel in this energy region but on the other hand, the γ + ^{27}Al data do not show this enhanced falloff. This is in contradiction to the RELDIS results and the deviation is well outside statistical and systematic uncertainties. RELDIS results also exhibit a steeper falloff for heavier nuclei (note that Fig. 3 shows γ + ^{40}Ca calculations). The enhanced production in heavier nuclei exhibited by the data taken in this experiment, may be due to an underestimation of the tail of the internal momentum distribution of the nucleons or a signal that coherent processes should be included in the model.

Another remark to Fig. 3 is that the π^+ cross-section in the γ + ^{2}H reaction does not follow the elementary $\gamma + p$ trend, but rather the trend established by the γ + nucleus reactions. It thus appears as if the presence of one single pn pair leads to the normal competition between the single nucleon and quasi-deuteron processes.

It should finally be stressed that in this near-threshold energy domain, the available phase-space for pion production becomes increasingly limited and a high detection threshold (e.g. 17 MeV at 90°) makes this restriction even more important.

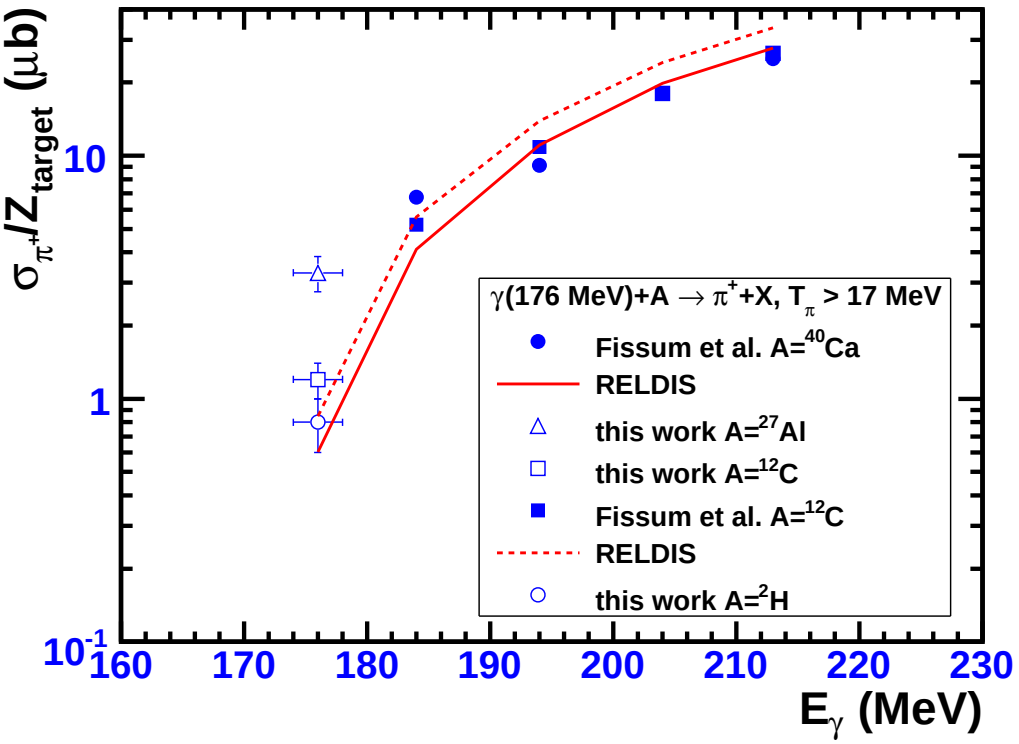

Fig. 3. Total yield of π^+ with $T_\pi > 17$ MeV (the pion-detection threshold from Ref. [11]) as a function of E_γ. Points represent data (this work and Ref. [11]) according to the legend and curves represent RELDIS calculations with a real pion potential of -20 MeV for the γ + ^{12}C (solid) and γ + ^{40}Ca (dashed) reactions. Systematic uncertainties of the measurements are given in Table 3. See text for details.

4.2 Angular distributions of produced π^+

In Fig. 3, the falloff of π^+ photoproduction at energies < 180 MeV was noted. Fig. 4 shows that the differential cross-section, $d\sigma/d\Omega$, decreases by a factor 4 - 7 if the detector limit is raised from 9 MeV (this experiment) to 17 MeV (detection threshold in Ref. [11]). The extrapolated increase in pion yield if the detection threshold could be lowered to 0 MeV, is a factor of 1.5 - 2. The trend exhibited by the data is reasonably well reproduced by RELDIS, with V_π = -20 MeV. Systematic uncertainties associated with the data points are are between 17% and 23% and the angular acceptance is ± 5.4° and ± 7.3° for the forward and 90° telescopes respectively.

This is also essentially true for the γ + ^{27}Al reaction, as shown in Fig. 5. The excess pion yield was here essentially found in the forward hemisphere. This fact goes hand-in-hand with the assumption of an extended internal

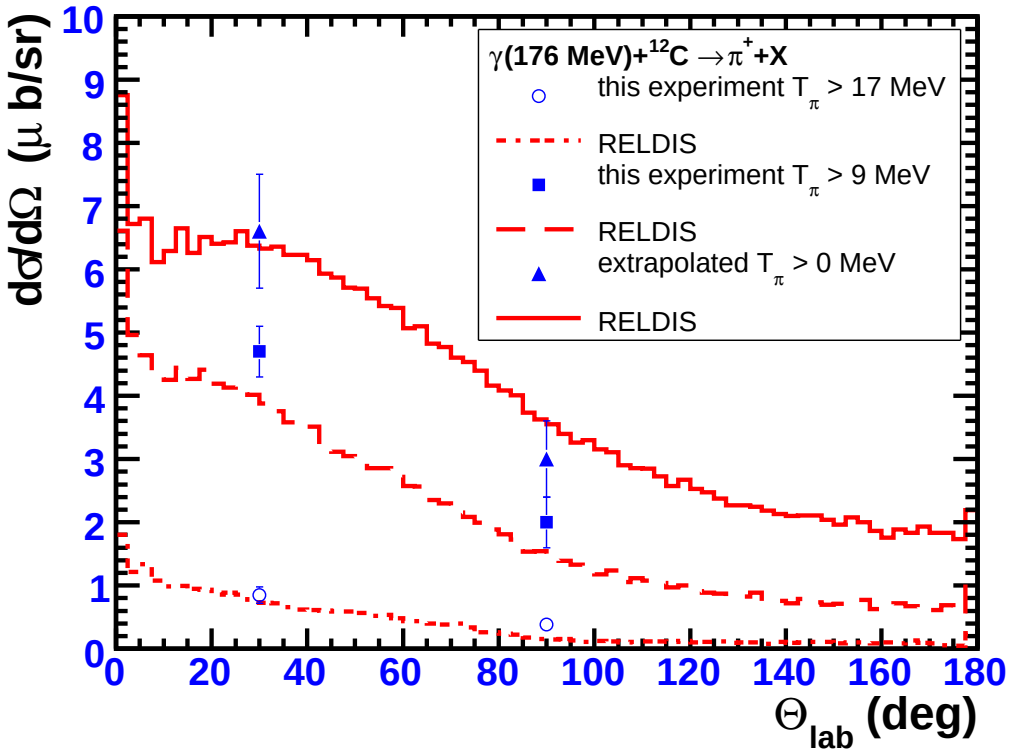

Fig. 4. Angular distributions of π^+ with $T_\pi > 17$ MeV (open points), > 9 MeV (squares) and > 0 MeV (triangles), emitted in γ + ^{12}C reactions at 176 MeV. Systematic uncertainties of the measurements are between 17 and 23%. Curves represent RELDIS calculations with a real pion potential of -20 MeV.

momentum distribution since the coupling of the relative momentum vector to the internal momentum vector produces a forward-focusing effect. However, there are other tentative explanations such as too strong reabsorption in the model that are plausible. Finally, we note again that the γ + ^{2}H reaction behaves more like the reaction on heavier nuclei than the elementary process.

4.3 Double-differential cross-section

The conclusion from the $d\sigma/d\Omega$ data of π^+ in γ + ^{12}C reactions (Fig. 4) was a slight underprediction by RELDIS with V_π = -20 MeV which, however, rather tends to become an overprediction when extrapolating the data to T_π = 0 MeV. The behaviour of the double differential cross-section as a function of pion kinetic energy (Fig. 6) at 30° and 90° makes the overestimation even more plausible. The obvious overprediction for low T_π is to some extent compensated by more extended high energy tails in the data.

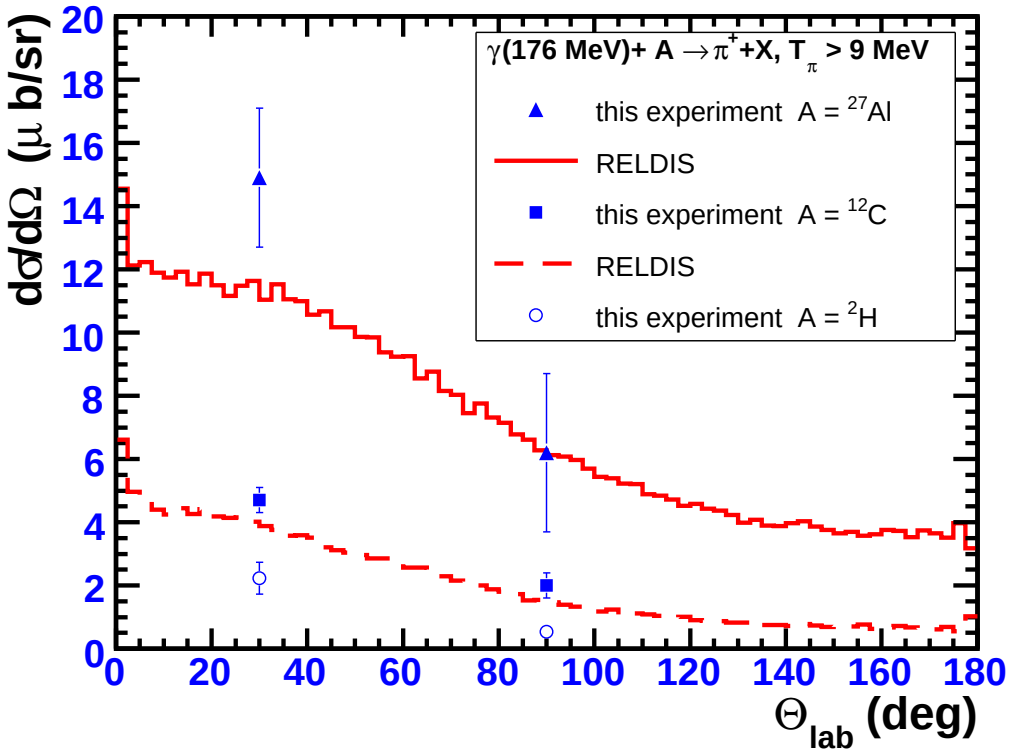

Fig. 5. Angular distributions of π^+ with $T_\pi > 9$ MeV in γ + A (see legend) reactions at 176 MeV. The systematic uncertainties are between 17% and 28%. The angular acceptance is $\pm$ 5.4° and $\pm$ 7.3° for the 30° and 90° respectively. Curves represent RELDIS calculations for A = ^{12}C (dashed) and A = ^{27}Al (solid) with a real pion potential of -20 MeV.

The same tendencies are more pronounced for the γ + ^{27}Al data (Fig. 7). In this case, RELDIS calculations exhibit no high-energy tail and the expected maximum in a Coulomb shifted spectrum of π^+ from the one-nucleon scattering process seems to fall at lower energies in the calculations. All calculated curves in Fig. 6 and 7 have a steep rise in the second bin, corresponding to an effective Coulomb barrier of $\sim$1 MeV. This appears to be too low, at least for the ^{27}Al case, where a more realistic Coulomb shift of 3 - 4 MeV would improve the comparison. The choice of the optimal pion potential may suffer from this mismatch. More data, especially on reactions with heavy targets, are however needed to set this question. At present it appears reasonable to believe that the potential falls in the interval -20 MeV to -15 MeV for light nuclei, with the lower value more representing ^{27}Al and the higher (-15 MeV) representing ^{12}C.

The form of the 30° energy spectrum of π^+ from γ + ^{2}H reactions (Fig. 7) is somewhat different in that the low energy point ($\sim$11 MeV) has a low

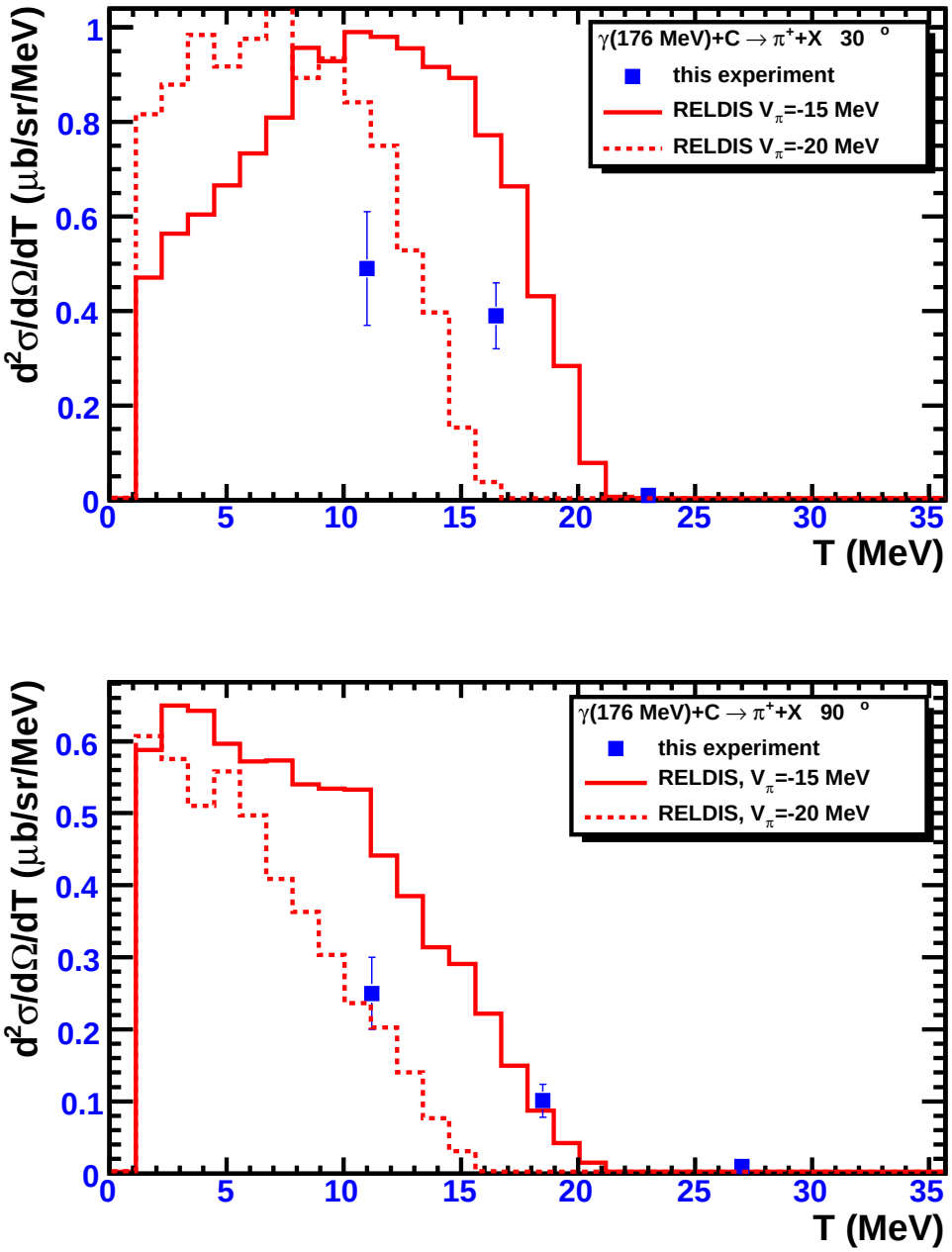

Fig. 6. Double-differential cross-section data for π^+ photoproduction with $T_\pi > 9$ MeV in $\gamma + {}^{12}C$ reactions at 176 MeV. The detector angle is 30° (upper panel) and 90° (lower panel). Note the experimental points at $T_\pi > 20$ MeV. Systematic uncertainties are between 20% and 25% and the uncertainty of the energy positions typically 1 MeV. Curves represent RELDIS calculations with a real pion potential of -20 MeV (dashed) or -15 MeV (solid).

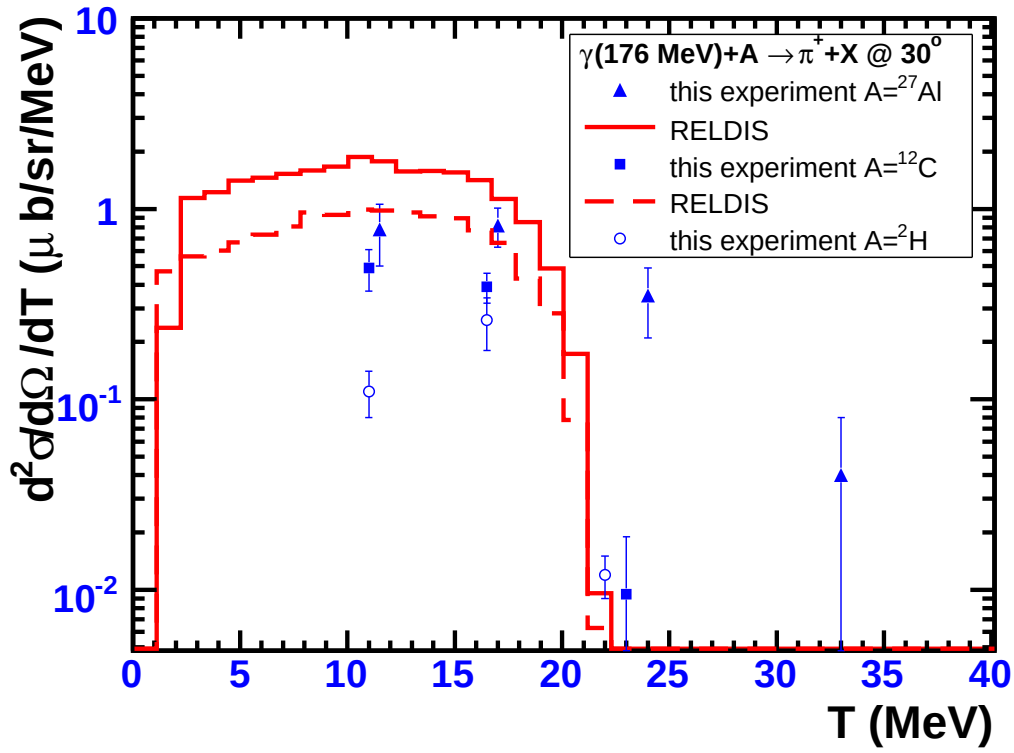

Fig. 7. Double-differential cross-section data for π^+ photoproduction detected at 30°, with $T_\pi > 9$ MeV in γ + ^{2}H,^{12}C and ^{27}Al (see legend) reactions at 176 MeV. Systematic uncertainties are between 22% and 28% and the uncertainy in energy position typically 1 MeV. Curves represent RELDIS calculations for Al and C reactions with a real pion potential of -20 MeV.

$d^2\sigma/d\Omega dT$ value. Even if this fact is significant, it must be stressed that the H_2 data are derived as a difference between the CH_2 target and C target data, which makes the systematic uncertainties larger, 26 - 28%, than for the other targets.

5 Conclusions

Near-threshold (γ,π) reactions in light nuclei may be described by an intranuclear cascade model like RELDIS. This means that the basic processes in RELDIS at these energies namely quasi-deuteron absorption and photon absorption on a single bound nucleon, should be dominant. Chosing depth of the real pion potential of -20 to -15 MeV results in RELDIS predictions which

match the data. Our approach to pion-nucleus reactions is similar to the one adopted in the Liege intranuclear cascade model [27], which was recently reconsidered in theoretical investigations of the average potential energy felt by a pion inside the nucleus. Our finding of V_π = -20 MeV agrees well with the values found in the literature [27], with a surface component of V_π between -5 and -25 MeV. Since low-energy pions, produced in the central part of a nucleus, are more easily absorbed than those produced close to the nuclear surface, it is relevant to use this surface component of V_π for the comparison.

The shapes of the experimental π^+ angular and (in particular) energy distributions differ from RELDIS predictions. Furthermore, the total π^+ yield in heavier nuclei is underestimated by the code by a large factor. Model particulars, such as the effective Coulomb potential, the exact form of the degenerate nucleon momentum distribution and the energy and density dependence of the pion potential could certainly be tuned to improve the comparison. The discrepancies also hint that multinucleon channels can play a role not only in pion absorption but also in pion production processes

π^+ cross-sections per proton are much higher in the elementary $\gamma + p$ reaction than in γ + nucleus reactions close to threshold. The fact that the γ + ^{2}H data follow the γ + nucleus trend indicates that the balance between quasi-deuteron absorption and single-nucleon absorption is achieved already for deuteron reactions. In fact, all data from this experiment indicate that the effects of the nuclear environment are small for nuclei with A < 30.

We look forward to studying the details of the pion production mechanism in forthcoming tagged (γ,π) experiments at MAX-lab at energies up to $\sim$220 MeV in the very near future.

6 Acknowledgements

The authors acknowledge the outstanding support of the MAX-lab staff during this challenging startup period at the upgraded Tagged Photon Facility. Funding of this work from the Swedish Research Council, the Knut and Alice Wallenberg Foundation and the U.S. Department of Energy is acknowledged.

References

[1] B. Krusche, Prog. Part. Nucl. Phys. **55** (2005) 46.

[2] A. Hombach, A. Engel, S. Teis et al., Z. Phys. A **352** (1995) 223.

[3] T. Kobayashi, K. Takeshita, A. Kagaya et al., J. Phys. Soc. Japan **58** (1989) 1570.

[4] K. Shoda, O. Sasaki, K. Takeshita et al., J. Phys. Soc. Japan **63** (1994) 478.

[5] J. Laget, Phys. Reports **69** (1981) 1.

[6] E. Khan, S. Goriely, D. Allard et al., Astropart. Phys. **23** (2005) 191.

[7] C. Scheidenberger, I. A. Pshenichnov, K. Summerer et al., Phys. Rev. C **70** (2004) 014902.

[8] J. O. Adler et al., Nucl. Instr. Methods **A388** (1996) 17.

[9] J. O. Adler, Proc. Second MAX-lab Workshop on the Nucl. Phys. Prog. with Real Photons below 250 MeV, Lund 2002, p. 73.

[10] J. O. Adler et al., Dept. of Nuclear Physics Photonuclear Group Report 01/01, LUNFD6/(NFFR-3086), 2001.

[11] K. Fissum, H. S. Caplan, E. L. Hallin et al., Phys. Rev. C **53** (1996) 1278.

[12] A. S. Iljinov, I. A. Pshenichnov, N. Bianchi et al., Nucl. Phys. **A616** (1997) 575.

[13] I. A. Pshenichnov, B. L. Berman, W. J. Briscoe et al., Eur. J. Phys. A. **24** (2005) 69.

[14] V. Bernard, J. Girard, J. Julien et al., Nucl. Phys. **A423** (1984) 511.

[15] http://geant4.web.cern.ch/geant4/

[16] C. G. Cross et al., Nucl. Phys. **A593** (1995) 463 and references therein

[17] T. Terasawa, K. Maeda and M. N. Thompson, Internal Report, Private Communication.

[18] J.L. Matthews, D.J.S. Findlay, S. N. Gardiner and R.O. Owens, Nucl. Phys. **A267** (1976) 51 and D.J.S. Findlay and R.O. Owens, Nucl. Phys. **A292** (1977) 53.

[19] M. Anghinolfi et al., Nucl. Phys. **A399** (1983) 66.

[20] H. Ruijter et al., Phys. Rev. C **54** (1996) 3076, and references therein

[21] J. S. Levinger, Phys. Rev. **84** (1951) 43.

[22] A. Leprêtre, H. Beil, R. Bergère, P. Carlos, J. Fagot, A. De Miniac and A. Veyssière, Nucl. Phys. **A367** (1981) 237.

[23] J. M. Laget, Nucl. Phys. **A312** (1978) 256.

[24] R. L. Walker, Phys. Rev. **182** (1969) 1729.

[25] W. J. Metcalf, R. L. Walker, Nucl. Phys. **B76** (1974) 253.

[26] P. Corvisiero, L. Mazzaschi, M. Ripani et al., Instr. and Meth. **A346** (1994) 433.

[27] Th. Aoust and J. Cugnon, Phys. Rev. C **74** (2006) 064607.